Mapping the interacting boson approximation symmetry triangle: New trajectories of structural evolution of rare-earth nuclei

E. A. McCutchan,[1] N. V. Zamfir,[1] and R. F. Casten[1,2]
[1]*WNSL, Yale University, New Haven, Connecticut 06520-8124, USA*
[2]*Institut für Kernphysik, Universität zu Köln, Köln, Germany*
(Received 18 February 2004; published 3 June 2004)

The discovery of a set of analytic solutions to describe nuclei at the critical point of spherical-deformed phase transitions has led to an increased interest in the properties of 0^+ excited states. This idea provides the motivation for the present investigation to determine sets of interacting boson model (IBA) parameters that reproduce the properties of all low-lying, positive-parity excitations, including the first excited 0^+ state, for a wide range of even-even, collective nuclei. Detailed fits of isotopic chains in the rare-earth region are shown to reproduce the energies of the positive-parity states and to provide a reasonable description of their transition matrix elements. Two neutron separation energies, isomer shifts, and isotope shifts are also described using a truncated IBA-1 Hamiltonian. A proposed set of polar coordinates allows for a mapping of these parameters into the IBA symmetry triangle and a comparison of trajectories for different isotopic chains.

DOI: 10.1103/PhysRevC.69.064306 PACS number(s): 21.10.Re, 21.60.Fw, 27.70.+q

I. INTRODUCTION

Over the last 25 years, a large number of interacting boson model (IBA) calculations have been performed, establishing that the model [1] is a valuable tool in understanding nuclear structure. One important feature of the IBA is its ability to describe the collective properties of nuclei spanning a large variety of structures with a single, simple Hamiltonian. This was first demonstrated by Scholten *et al.* [2] in a study of the Sm isotopic chain using a simplified Hamiltonian. Further phenomenological studies have been carried out using the full SU(6) Hamiltonian to describe chains of nuclei ranging from Ba to U (see, e.g., Refs. [3,4]) or using a truncated Hamiltonian to describe the Ru and Pd isotopes [5] and the $Z=50$ to 82 shell [6].

Recently, with the introduction of dynamical symmetries, E(5) (Ref. [7]) and X(5) (Ref. [8]), to describe nuclei at the critical points of second- and first-order phase transitions, respectively, and with supporting evidence [9,10] that some nuclei exhibit structures very close to these paradigms, more attention has been focused on the low-lying excited 0^+ states. Previous IBA-1 calculations [6] gave significant deviations from the data in their predictions for the lowest 0^+ excited sequences. This is perhaps not surprising since excited 0^+ states have long proved difficult to understand. The recent emphasis on the first excited 0^+ sequence, which is one of the key signatures in the E(5) and X(5) models, and the success of these models in accounting for their properties, suggest that it might be possible to determine a set of parameters within the framework of the IBA-1 which reproduce the properties of all low-lying, positive-parity excitations.

Using a simplified, two-parameter Hamiltonian, the energies, electromagnetic transitions, two neutron separation energies, and isomer and isotope shifts are calculated for several rare-earth isotopic chains. The evolution of the resulting parameters and observables is then analyzed over a wide range of structures. From the parameters obtained, a mapping of each isotopic chain in the IBA parameter space is illustrated in the IBA symmetry triangle using a simple set of polar coordinates.

II. DESCRIPTION OF METHOD

Calculations were performed in the framework of the IBA-1 (where no distinction is made between protons and neutrons) using the extended consistent Q formalism (ECQF) [11] with the Hamiltonian [12,13]

$$H(\zeta) = c\left[(1-\zeta)\hat{n}_d - \frac{\zeta}{4N_B}\hat{Q}^\chi \cdot \hat{Q}^\chi\right], \tag{1}$$

where

$$\hat{Q}^\chi = (s^\dagger \tilde{d} + d^\dagger s) + \chi(d^\dagger \tilde{d})^{(2)} \tag{2}$$

and $\hat{n}_d = d^\dagger \cdot \tilde{d}$.

The same quadrupole operator is used in the Hamiltonian and the E2 operator, which is given by

$$T(\mathrm{E2}) = e_B Q, \tag{3}$$

where e_B represents the boson effective charge.

The Hamiltonian of Eq. (1) involves two parameters, ζ and χ (c is a scaling factor). The boson number N_B is given by half the number of valence protons and neutrons, each taken separately relative to the nearest closed shell. In this analysis, N_B is obtained relative to the standard magic numbers 50, 82, and 126.

The parameter space for this Hamiltonian is traditionally represented by a triangle [14] with one IBA dynamical symmetry at each vertex. Figure 1 illustrates the IBA symmetry triangle with the three dynamical symmetries in terms of the Hamiltonian parametrization in Eq. (1). In this parametrization, the three symmetries are given by $\zeta=0$, any χ for U(5), $\zeta=1$, $\chi=-\sqrt{7}/2$ for SU(3), and $\zeta=1$, $\chi=0$ for O(6). Transition regions between the three symmetries can be described by numerical diagonalizations of the above Hamiltonian [Eq. (1)] for intermediate parameter values.

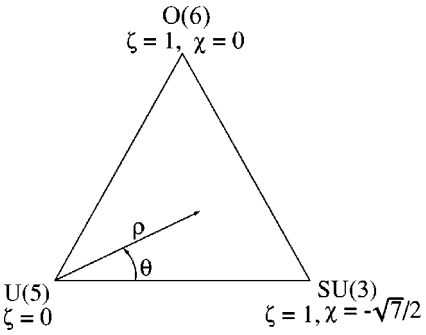

FIG. 1. The IBA symmetry triangle. Symmetry limits are given in terms of the parametrization of the Hamiltonian in Eq. (1). Also included is an illustration of the polar coordinates ρ and θ as defined in Eq. (8).

Generally, the overall structure of a typical collective even-even nucleus can be interpreted by taking into account a few key observables. Considered in the fits was basic information on the ground, 0_2^+, and quasi-2_γ^+ bands. In terms of the energies, emphasis was placed on the ratios: $R_{4/2} \equiv \mathrm{E}(4_1^+)/E(2_1^+)$, $\mathrm{E}(0_2^+)/\mathrm{E}(2_1^+)$, and $\mathrm{E}(2_\gamma^+)/\mathrm{E}(2_1^+)$, where the 2_γ^+ state is a member of the two-phononlike multiplet in vibrational nuclei or else the bandhead of the quasi-γ band in rotational nuclei. For the electromagnetic transition probabilities, the B(E2) ratio, $B_{2\gamma}=\mathrm{B(E2};2_\gamma^+\rightarrow 0_1^+)/\mathrm{B(E2};2_1^+ \rightarrow 0_1^+)$, as well as the branching ratio, $R_{2\gamma}=\mathrm{B(E2};2_\gamma^+ \rightarrow 0_1^+)/\mathrm{B(E2};2_\gamma^+\rightarrow 2_1^+)$, were considered. These observables were chosen because they involve bandheads that are easy to identify and are measured precisely enough to allow for a useful comparison.

Parameters for each nucleus were determined by considering contour plots [6] of the above five observables. In almost all cases, with exceptions discussed below, a small range of parameters is able to reproduce the experimental energy ratios $R_{4/2}$, $\mathrm{E}(0_2^+)/\mathrm{E}(2_1^+)$, and $\mathrm{E}(2_\gamma^+)/\mathrm{E}(2_1^+)$, to within 5%. This result is in contrast to previous fits in this region [6], where the same Hamiltonian of Eq. (1) was used; however, less emphasis was placed on reproducing the energy of the first excited 0^+ state so that, generally, the calculations differed from the experimental 0_2^+ energy, in some cases, by several hundred keV. In addition to a reduced emphasis on fitting the 0_2^+ state, the previous fit [6] of this region kept the strength of the quadrupole-quadrupole interaction strictly constant. In the present work, this strength was allowed to vary and it was found to be approximately constant for large boson numbers ($N_B \geqslant 10$), but reduced in the vibrational limit, as would be expected in order to reproduce spectra close to the U(5) limit. Since the above ratios $R_{2\gamma}$ and $B_{2\gamma}$ can involve weak or forbidden transitions, less stringent agreement between the measured values and calculations was required than for the energy observables. Considering that the B(E2) value for the $2_\gamma^+\rightarrow 0_1^+$ transition is on the order of a few percent of the value for the collective $2_1^+\rightarrow 0_1^+$ transition, agreement of the calculations of $B_{2\gamma}$ within a factor of ~ 2 was taken as acceptable.

For both the energies and electromagnetic transition probabilities, a scaling factor is involved: $H=cH_o$ for the Hamiltonian and $T(\mathrm{E2})=e_B Q$ for the quadrupole operator. Since the parameters were obtained from ratios of energies or electromagnetic transitions, ζ and χ are independent of the scaling factors c and e_B. The scaling factor c in the energies was chosen to normalize the predictions to the experimental 2_1^+ level energy. The effective charge e_B was determined by normalizing the predictions to the experimental $\mathrm{B(E2};2_1^+\rightarrow 0_1^+)$ values; it varied only slightly from nucleus to nucleus, ranging from values of 0.13 eb to 0.15 eb.

For some nuclei, some of the above observables [$R_{2\gamma}$, $B_{2\gamma}$, or $\mathrm{E}(0_2^+)$] are not known. In a few nuclei, only $\mathrm{E}(2_1^+)$ and $R_{4/2}$ are known, which does not sufficiently constrain ζ and χ. For these nuclei, the choice of parameters was based on reproducing the known observables while at the same time attempting to follow the trend of parameters in neighboring nuclei.

Traditionally, the focus of IBA calculations is on reproducing energy spectra or electromagnetic transitions, often ignoring the description of other important quantities that can be calculated with the model. Calculations of binding energies $\mathrm{BE}(N_B)$ can provide a sensitive test of the Hamiltonian used to fit entire chains [15,16] and can aid in distinguishing between apparently equivalent descriptions of energy spectra and electromagnetic transitions. In this work, two neutron separation energies S_{2n}, given by

$$S_{2n} = \mathrm{BE}(N_B) - \mathrm{BE}(N_B - 1), \tag{4}$$

are also analyzed for each isotopic chain. In order to calculate binding energies on an absolute scale, terms related to the global Hamiltonian [linear and quadratic U(6) Casimir operators] must be added to the Hamiltonian given in Eq. (1). In calculating two neutron separation energies, this translates into an additional contribution which is linear in the number of bosons

$$S'_{2n} = \mathcal{A} + \mathcal{B}N_B + \mathrm{BE}(N_B) - \mathrm{BE}(N_B - 1), \tag{5}$$

with the coefficients $\mathcal{A}$ and $\mathcal{B}$ taken as constant across an isotopic chain [15].

Other quantities that are often absent from IBA calculations involve nuclear radii, which are easily calculated using the electric monopole operator. Within the rare-earth region, past calculations [2,17] have focused only on the Sm isotopic chain. Two quantities related to differences in nuclear radii, isomer and isotope shift, can act as a sensitive probe of the structure of the nucleus since they are expected to change rapidly in transitional regions. Both quantities are related to the expectation value of the number of d bosons [18] and in transitional regions can reveal the character of the transition [19].

The isomer shift $\delta\langle r^2\rangle$ is a measure of the change in nuclear radius between the first 2_1^+ state and the ground state and is proportional to the difference in the expectation value of the number of d bosons $\langle n_d\rangle$ in the two states [18]:

$$\delta\langle r^2\rangle = \langle r^2\rangle_{2_1^+} - \langle r^2\rangle_{0_1^+} = \beta[\langle n_d\rangle_{2_1^+} - \langle n_d\rangle_{0_1^+}]. \tag{6}$$

In connecting the data to the calculations, the only parameter is β, which acts simply as a scaling factor.

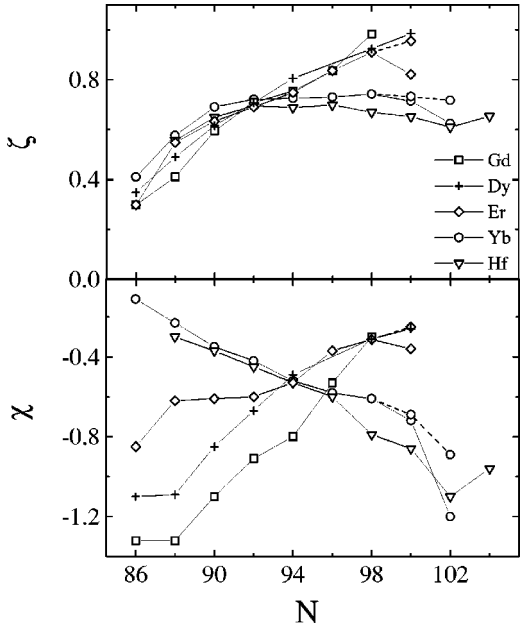

FIG. 2. Evolution of the parameters ζ and χ for the Gd-Hf isotopes as a function of increasing neutron number. Dashed lines correspond to parameters obtained when considering the experimental 0_3^+ state as the first collective excited 0^+ state.

The isotope shift $\Delta\langle r^2\rangle$ is a measure of differences in radii in the ground state between nuclei one neutron pair away from each other. In the IBA, it contains, in addition to the term proportional to n_d, a contribution from the core, independent of the structure of the nucleus [18], given by

$$\Delta\langle r^2\rangle^{(N)} = \langle r^2\rangle_{0_1^+}^{(N+2)} - \langle r^2\rangle_{0_1^+}^{(N)} = \gamma + \beta[\langle n_d\rangle_{0_1^+}^{(N+2)} - \langle n_d\rangle_{0_1^+}^{(N)}], \tag{7}$$

where, in the IBA-1 model, β is the same quantity as in the expression for the isomer shift in Eq. (6) and γ is the contribution from the core, which is the same for the entire region.

III. APPLICATION TO THE RARE-EARTH NUCLEI

Considered in the fits were collective even-even nuclei ($R_{4/2} \geqslant 2.0$) in the rare-earth region with $Z=64$ to 72 and $N=86$ to 104. In all, 40 nuclei are included in this survey. The data were taken from the Nuclear Data Sheets [20] with a cutoff date at the end of 2001, except where noted.

The parameters ζ and χ obtained for each nucleus are summarized in Fig. 2 and are given explicitly in Table I. Overall, the evolution of both parameters is relatively smooth, as would be expected in order to describe the gradual change in structure as boson number is varied. However, for some isotopic chains, there is a deviation in the evolution of the parameters, typically as they approach midshell. In some cases, this change could be an indication of an intruder structure, which will be discussed in more detail below. Typically, ζ increases as boson numbers increase and the nuclei evolve from vibrational to rotational, as expected. This trend is observed for all isotopic chains up to $N=92$.

TABLE I. Parameters ζ and χ for each isotopic chain as obtained in the present work.

Isotope	N	N_B	ζ	χ
Gd	86	9	0.30	−1.32
	88	10	0.41	−1.32
	90	11	0.59	−1.10
	92	12	0.72	−0.86
	94	13	0.75	−0.80
	96	14	0.84	−0.53
	98	15	0.98	−0.30
Dy	86	10	0.35	−1.10
	88	11	0.49	−1.09
	90	12	0.62	−0.85
	92	13	0.71	−0.67
	94	14	0.81	−0.49
	96	15	0.92	−0.31
	98	16	0.98	−0.26
Er	86	9	0.30	−0.85
	88	10	0.55	−0.62
	90	11	0.63	−0.61
	92	12	0.69	−0.60
	94	13	0.75	−0.53
	96	14	0.84	−0.37
	98	15	0.91	−0.31
	100	16	0.82	−0.36
	100[a]	16	0.96	−0.25
Yb	86	8	0.41	−0.11
	88	9	0.58	−0.23
	90	10	0.69	−0.35
	92	11	0.72	−0.42
	94	12	0.73	−0.52
	96	13	0.73	−0.58
	98	14	0.74	−0.61
	100	15	0.70	−0.75
	100[a]	15	0.73	−0.69
	102	16	0.62	−1.20
	102[a]	16	0.72	−0.89
Hf	88	8	0.56	−0.30
	90	9	0.65	−0.37
	92	10	0.70	−0.45
	94	11	0.69	−0.53
	96	12	0.70	−0.60
	98	13	0.67	−0.79
	100	14	0.66	−0.84
	102	15	0.61	−1.10
	104	16	0.65	−0.96

[a]Parameters were obtained by considering the second excited 0^+ state as the first collective 0^+ state.

For $N>92$, the Gd, Dy, and Er nuclei are described by an increasing ζ, while for Yb and Hf, ζ remains relatively constant up to midshell. The different trends in the evolution of parameters for various isotopic chains is even more pronounced for the parameter χ, with a clear separation into two distinct groups. For the Gd and Dy nuclei, the absolute value of χ starts out large for vibrational nuclei and gradually approaches -0.2 as N increases. A completely opposite trend is exhibited in the Yb and Hf chains, where χ is close to zero for vibrational nuclei and then grows towards the SU(3)

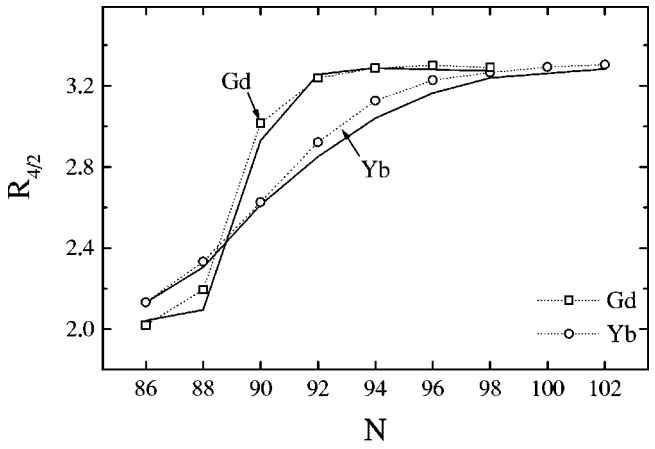

FIG. 3. Evolution of experimental (symbols with dashed lines) and calculated (solid lines) $R_{4/2}$ values for the Gd and Yb isotopes as a function of increasing neutron number.

value of −1.32 as neutron number approaches midshell. The evolution of parameters for the Yb and Hf chains is drastically different from previous fits in this region [6], and is a consequence of treating the 0_2^+ state equally with the 2_γ^+ state, as will be discussed in more detail below.

A fundamental observable to describe the structure of a nucleus is the $R_{4/2} \equiv \mathrm{E}(4_1^+)/\mathrm{E}(2_1^+)$ energy ratio. For the nuclei included in this study, all chains begin as vibrational with $R_{4/2}$ near 2.0 and move towards rotational ($R_{4/2} \rightarrow 3.33$) as neutron number is increased. This behavior is illustrated in Fig. 3 using the Gd and Yb chains as examples. For the Gd chain, the change in $R_{4/2}$ is quite sharp, while for the Yb isotopes, the evolution is much more gradual. The calculations reproduce these behaviors.

The calculated energy spectra are compared with the available experimental data for a sample of nuclei in Fig. 4, including examples of vibrational (^{156}Er, $R_{4/2}=2.3$), transitional (^{154}Gd, $R_{4/2}=3.0$), and rotational (^{160}Gd and ^{172}Yb, $R_{4/2}=3.3$) nuclei. As expected, the calculations provide a reasonable description of the low-lying spectra for a wide range of structures. All calculations for both the transitional and rotational spectra show a systematic underprediction of the moment of inertia of the excited 0_2^+ sequence, resulting in an expansion of the band compared with the experimental sequence. The quasi-γ band is reproduced well in all structures, with a slight overprediction in the energy spacings. One interesting feature is that two good rotational nuclei,

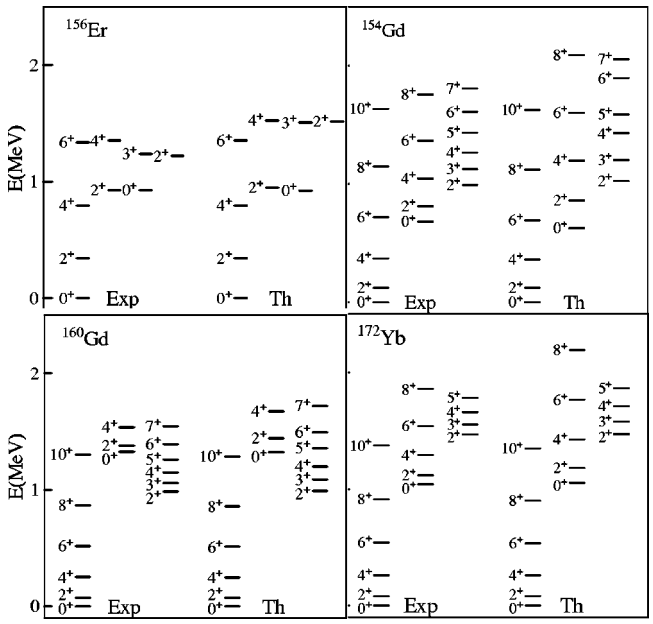

FIG. 4. Comparison of calculated and empirical energy levels for some rare-earth nuclei.

^{160}Gd and ^{172}Yb, are fit with strikingly different χ values (−0.5 and −1.2, respectively). This is due to the very different relative energies of the 0_2^+ and γ bands. The γ band is significantly lower than the 0_2^+ band in ^{160}Gd and significantly higher in ^{172}Yb. It is well known [21,22] that the γ band is lowered as χ deviates from the SU(3) value of −1.32 and that reversing the order of these bands [i.e., $\mathrm{E}(2_\gamma^+) > \mathrm{E}(0_2^+)$] requires χ values near SU(3) and significant coefficients of the n_d term in Eq. (1) (see contour plots of Refs. [6,11]).

A comparison of the systematics of experimental and calculated energies of key states for the Gd-Hf isotopic chains is given in Fig. 5. The overall agreement is excellent, with the calculations almost always agreeing with the experimental energies to within 5% or better. The most obvious discrepancies occur when there is a large energy separation between the 2_γ^+ and 0_2^+ levels (Dy and Er with $N=98$). In looking at the evolution of these two levels as a function of N, again the isotopic chains exhibit two different behaviors. For $N>90$, the energy of the 2_γ^+ state remains constant or decreases as N increases for the Gd, Dy, and Er nuclei, while undergoing a gradual increase in the Yb and Hf chains. This behavior is

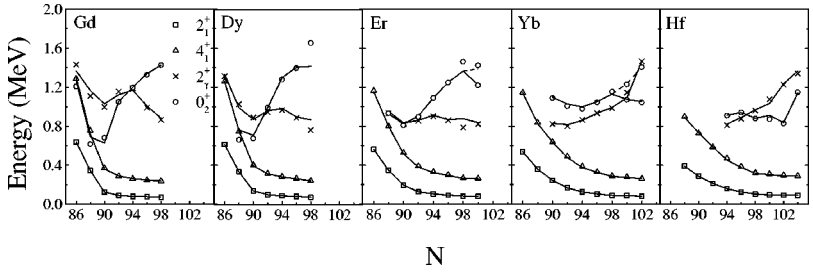

FIG. 5. Comparison of experimental level energies (symbols) and IBA calculations (solid lines) for the 2_1^+, 4_1^+ members of the ground band and the heads of the 2_γ^+ and 0_2^+ bands for the Gd, Dy, Er, Yb, and Hf isotopes. Data are taken from Ref. [20], except for ^{162}Yb taken from Ref. [29]. Dashed lines correspond to fits considering the experimental 0_3^+ state as the first collective excited 0^+ state.

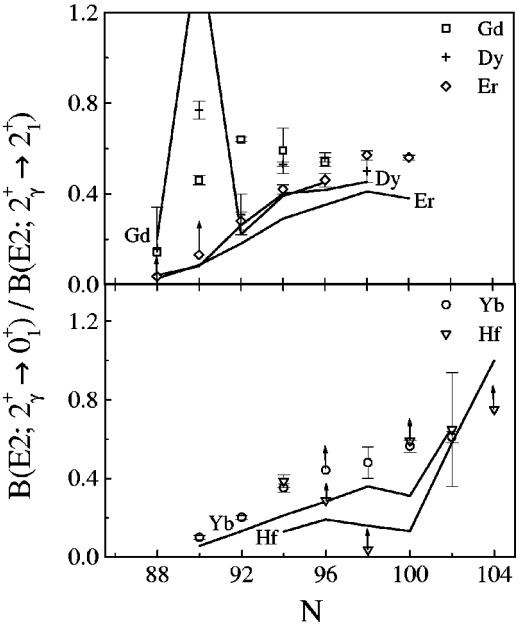

FIG. 6. Experimental $R_{2\gamma}=\mathrm{B(E2;}2^+_\gamma\rightarrow 0^+_1)/\mathrm{B(E2;}2^+_\gamma\rightarrow 2^+_1)$ ratios (symbols) compared with the IBA calculations (solid lines). For cases where δ is not measured, limits are represented by arrows.

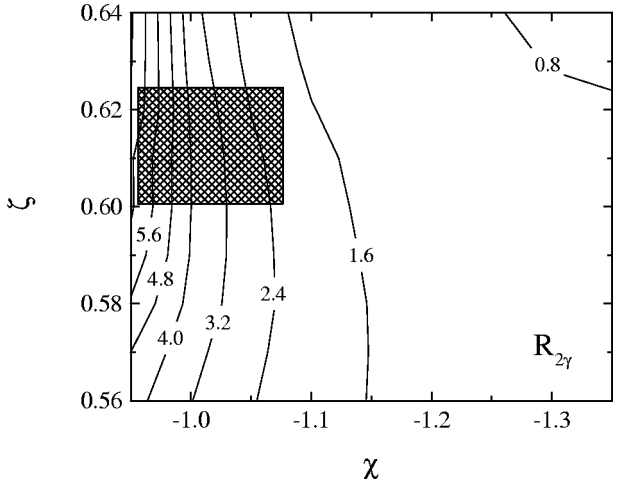

FIG. 7. Contour plot of the observable $R_{2\gamma}=\mathrm{B(E2;}2^+_\gamma\rightarrow 0^+_1)/\mathrm{B(E2;}2^+_\gamma\rightarrow 2^+_1)$ in the ζ,χ plane for $N_B=11$. The cross-hatched square area indicates the choice of parameters that reproduce the experimental energies of low-lying excitations in ^{154}Gd.

reversed when considering the evolution of the 0^+_2 state. For Gd, Dy, and Er, $E(0^+_2)$ gradually increases as N increases, while for the Yb and Hf nuclei, it remains relatively constant.

The evolution of the excited 0^+_2 states in the Er and Yb chains for $N\geqslant 100$ suggests the possibility of an intruder structure. As illustrated in Fig. 5, there is a clear change in the trend of the first excited 0^+ state energy for Er with $N=100$ and Yb with $N=100$, 102. A discontinuity in the trend of the parameters is also observed (Fig. 2) for the above nuclei. By considering the second experimental excited 0^+ state as the first collective excited 0^+ state in the IBA space, both energies and parameters follow a much smoother trend as indicated by the dashed lines in Figs. 2 and 5. More data are necessary to establish which experimental excited 0^+ state corresponds to the collective IBA state.

Another sensitive structural quantity is the ratio $R_{2\gamma}=\mathrm{B(E2;}2^+_\gamma\rightarrow 0^+_1)/\mathrm{B(E2;}2^+_\gamma\rightarrow 2^+_1)$, which is zero in the U(5) and O(6) limits and increases to the Alaga ratio of 0.7 in the rotational limit for large N_B. As shown in Fig. 6, the overall experimental trend is reproduced by the calculations. However, the values are, in general, underestimated by the model. There are also some nuclei for which it is not possible to find a consistent set of parameters to reproduce both the energy levels as well as this branching ratio. The most obvious case is ^{154}Gd, where the predicted ratio spikes well above any reasonable value. It is worth noting that a similar problem was encountered in fitting ^{154}Gd by the authors of Ref. [11]. Figure 7 illustrates a contour plot of the ratio $R_{2\gamma}$ with $N_B=11$ for a range of parameter values including the best fit for all observables. The crosshatched square region indicates the locus of parameter values where the experimental energy ratios $R_{4/2}$, $E(2^+_\gamma)/E(2^+_1)$, and $E(0^+_2)/E(2^+_1)$ are reproduced to within 5%. In this region, the model predicts only very large values (>1) for $R_{2\gamma}$. More realistic values (<0.8) for $R_{2\gamma}$ are obtainable with a different choice of parameters (i.e., $|\chi|\sim 1.32$ and $\zeta>0.64$); however, these parameters result in energies for the 2^+_γ and 0^+_2 states that differ by >600 keV from the experimental values.

Other branching ratios, such as $\mathrm{B(E2;}3^+_\gamma\rightarrow 4^+_1)/\mathrm{B(E2;}3^+_\gamma\rightarrow 2^+_1)$, are reproduced well using the parameters chosen in the method descibed above. This quantity goes to infinity in both the U(5) and O(6) limits and to the Alaga ratio of 0.4 in the SU(3) limit. As shown in Fig. 8, the calculations follow the expected trend of the data and also reproduce well the individual experimental ratios.

In considering the above observables, the level of agreement between theory and experiment was basically the same

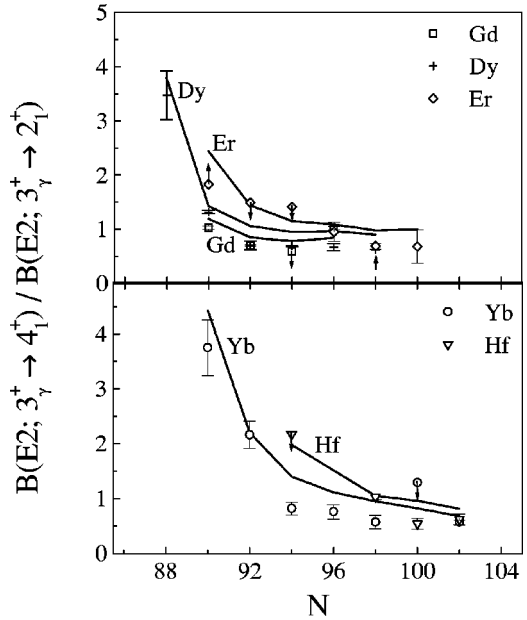

FIG. 8. Experimental $\mathrm{B(E2;}3^+_\gamma\rightarrow 4^+_1)/\mathrm{B(E2;}3^+_\gamma\rightarrow 2^+_1)$ ratios (symbols) compared with the IBA calculations (solid lines). For cases where δ is not measured, limits are represented by arrows.

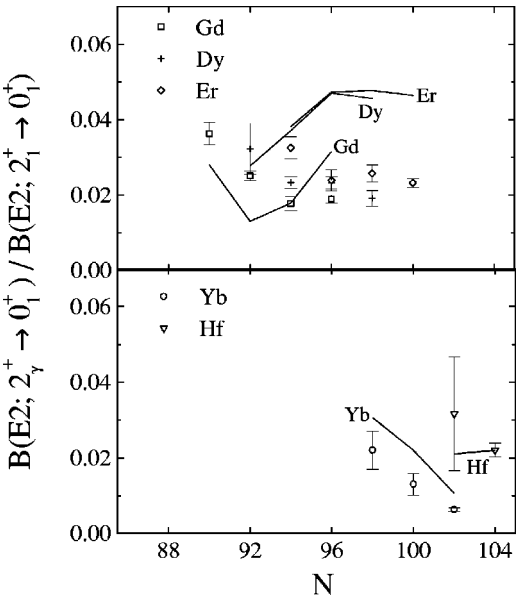

FIG. 9. Experimental $B_{2\gamma}=B(E2;2^+_\gamma \rightarrow 0^+_1)/B(E2;2^+_1 \rightarrow 0^+_1)$ ratios (symbols) compared with the IBA calculations (solid lines).

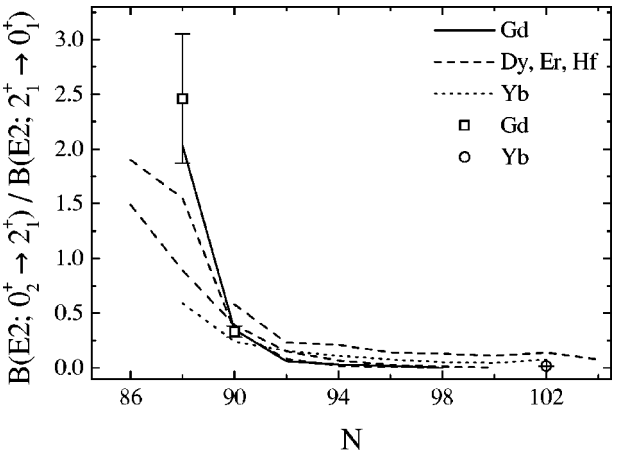

FIG. 10. Experimental $B(E2;0^+_2 \rightarrow 2^+_1)/B(E2;2^+_1 \rightarrow 0^+_1)$ ratios (symbols) compared with the IBA calculations (lines).

for all isotopic chains. This is not the case, however, for all observables. Consider, for example, the ratio $B_{2\gamma}=B(E2;2^+_\gamma \rightarrow 0^+_1)/B(E2;2^+_1 \rightarrow 0^+_1)$, illustrated in Fig. 9. Considering that the numerator is either a forbidden or interband transition, while the denominator is a collective intraband transition, this quantity is expected to be small. For all isotopic chains, the theory provides reasonable agreement, with predictions no larger than 0.05, which is the same range as seen in the data. For the Yb and Hf isotopic chains, the individual values are well reproduced. In the Gd, Dy, and Er isotopes, however, detailed agreement is obtained only for a few vibrational isotopes, while the trend for increasing N is not reproduced and, by the middle of the shell, the calculations diverge from the data by a factor of ~ 2.

Having obtained a reasonable fit to the energies of the 0^+_2 states, it is appropriate to consider transitions from these state as well. Unfortunately, the relevant experimental data are sparse, with only three known absolute $B(E2;0^+_2 \rightarrow 2^+_1)$ values in this region. The calculations for the ratio $B(E2;0^+_2 \rightarrow 2^+_1)/B(E2;2^+_1 \rightarrow 0^+_1)$ for all isotopic chains are shown in Fig. 10 and are compared with the known data. Perhaps not surprisingly, all the curves follow the same trend (large for small N then decreasing to zero as N increases) since the numerator is allowed in the U(5) limit and forbidden in the SU(3) limit. Interesting though, is that the calculations (spanning a wide range of structures) are in excellent detailed agreement with the experimental values.

In addition to reproducing the properties of the low-lying excitations, the fit parameters obtained in this work also reproduce well the properties of the yrast states. Using Dy as an example, the yrast energies and B(E2) values up to spin 10^+ are compared to the predictions in Fig. 11. Perfect agreement corresponds to a point that lies exactly on the diagonal; most of the energies lie very close to this line and the B(E2) values are usually within 2σ of the diagonal line.

As mentioned previously, while the energies and electromagnetic transition properties are reproduced reasonably by the fit parameters, a sensitive test of the applicability of the Hamiltonian to the entire isotopic chain can be achieved by considering two neutron separation energies. It has been shown [16] that it is possible to find parameters that predict well the experimental energy spectra yet differ significantly from the experimental data in their predictions of two neutron separation energies. The results of the calculations of S'_{2n} for the Gd and Yb chains are given in Fig. 12, using the additional constants (given in MeV) $\mathcal{A}=17.23$, $\mathcal{B}=-0.670$ for Gd and $\mathcal{A}=20.35$, $\mathcal{B}=-0.581$ for Yb. A reasonable description is obtained for both the nonlinear behavior of the Gd chain and the linear behavior of the Yb chain. The nonlinearity in the S'_{2n} behavior of the Gd chain is similar to that observed for the Sm isotopic chain [2] and, in fact, Gd mirrors Sm in the evolution of many basic observables. It has been suggested [23] that a flatness in the S'_{2n} evolution is

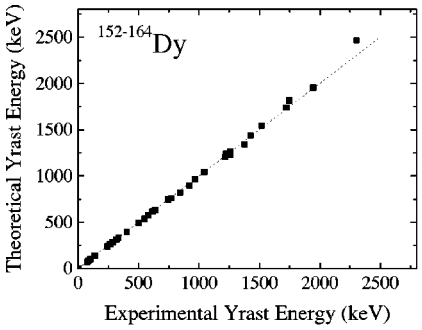

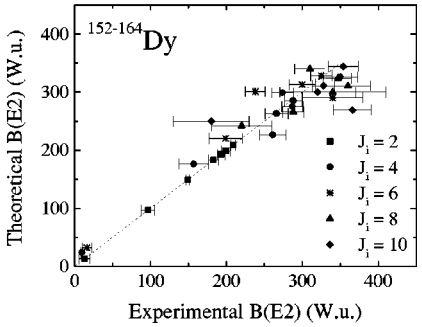

FIG. 11. Theoretical versus experimental (a) yrast energies and (b) B(E2) values for $^{152-164}$Dy up to spin 10^+. The dashed line corresponds to an exact agreement between experiment and theory.

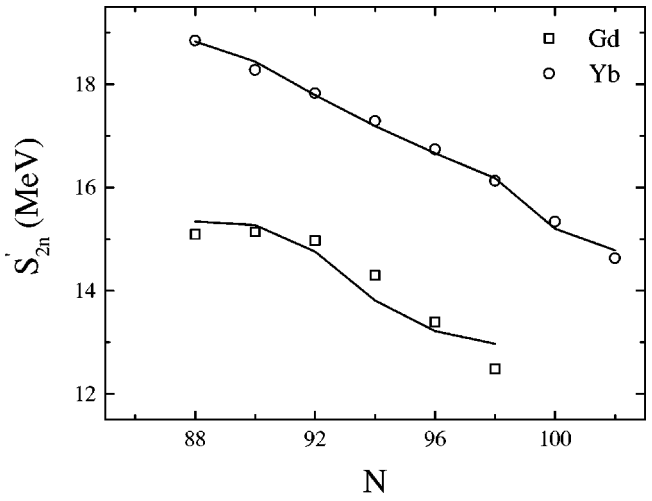

FIG. 12. Two neutron separation energies for the Gd and Yb isotopes (symbols) compared with the IBA calculations (solid lines).

evidence of a first-order phase transition. Previous studies of other properties of the Sm and Gd chains have found that these nuclei undergo such a transition [12].

The isomer shift $\delta\langle r^2\rangle$ is expected to change dramatically in the transitional region, going from β in U(5) to $\beta/(2N_B-1)$ in SU(3) [18], which results in an order of magnitude difference. As is shown in Fig. 13(a), this large drop has been observed experimentally in the Gd chain and is reproduced well by the calculations, taking $\beta=0.03$ fm^2. Again, the behavior for Gd resembles that of Sm [2] and is once more an indication of a first-order phase transition [19]. While no experimental data are available for the Dy, Er, or Yb chains, the calculations are given in Fig. 13(b) using the same β as for Gd. Notice the decreased sharpness of the transition from large values of $\delta\langle r^2\rangle$ to small values for increasing Z.

In the evolution of $R_{4/2}$, S'_{2n}, and $\delta\langle r^2\rangle$, a strong similarity now emerges. For each of these quantities, there is a sharp evolution as a function of N for the Gd isotopes, and a more gradual evolution as N varies for the Yb chain. This behavior will be important to the discussion of trajectories in the triangle in the next section.

In Fig. 13(c), the results of the calculation of the isotope shift $\Delta\langle r^2\rangle^{(N)}$ are compared with the available experimental values for Gd. Taking $\beta=0.03$ fm^2 from the fit to the isomer shift data and $\gamma=0.15$ fm^2 gives predictions which reproduce the data for $N\geqslant 90$ well, but do not reproduce the sharp spike that occurs at $N=88$. In order to better reproduce the jump in $\Delta\langle r^2\rangle^{(N)}$ that occurs at $N=88$, a large $\beta(=0.15$ fm$^2)$ and no γ term are necessary. However, using a β of 0.15 fm^2 in the isomer shift calculations would shift the results by a factor of 5, leading to a gross overprediction of the experimental data. This creates an obvious discrepancy, since the IBA-1 parameter β in Eqs. (6) and (7) might be expected to be the same. This discrepancy in β values could be due to the different contributions to the isomer and isotope shifts of the valence protons and neutrons which, obviously, is not considered in the IBA-1 model. Indeed, fits [24–26] using the IBA-2, where a distinction is made between valence protons and neutrons, require different values for the proton and neutron components of β in fitting isomer and isotope shift data.

The data and predictions for $\Delta\langle r^2\rangle^{(N)}$ are given for the Dy, Er, and Yb chains in Fig. 13(d). The predicted values are calculated using the same β and γ parameters (0.15 fm^2 and 0, respectively) taken from the best fit to the Gd isotope shift data. Again, there is a decreased sharpness with increasing Z, both in the predictions and the data, for the spike observed at $N=88$. The combination of both the discontinuity of $\Delta\langle r^2\rangle^{(N)}$ at $N=88$ and its decreasing sharpness with increasing Z is evocative of the behavior of both the two neutron separation energies and isomer shifts. Since both S'_{2n} and $\delta\langle r^2\rangle$ can provide an indication of a first-order phase transition, their similarities with the isotope shift behavior suggest that the discontinuity at $N=88$ in $\Delta\langle r^2\rangle^{(N)}$ could also point to a signature of a first-order phase transition.

From the above discussion, it is apparent that these isotopes tend to group into two classes, the Gd, Dy, and Er

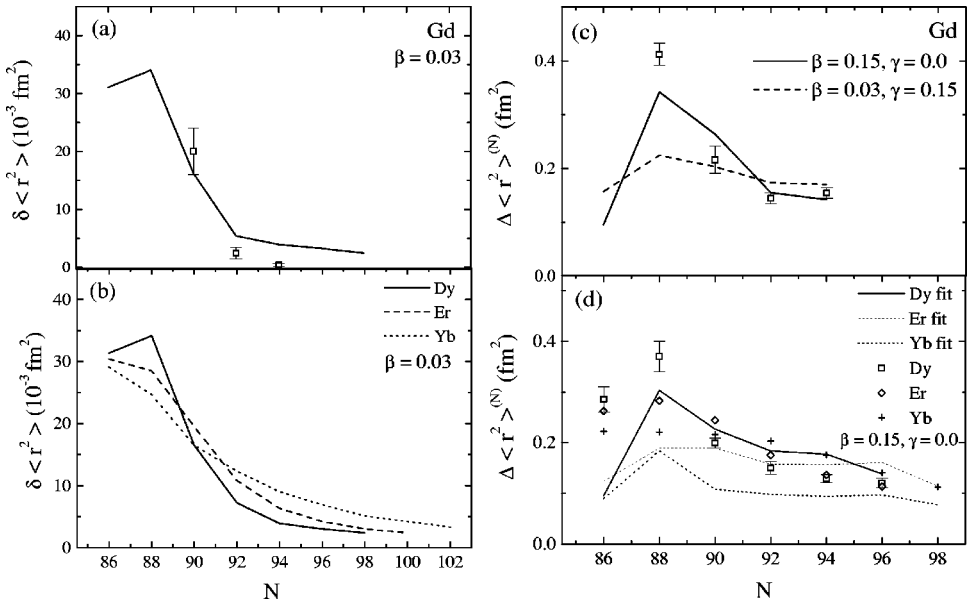

FIG. 13. Experimental values (symbols) and calculations (lines) of isomer and isotope shifts. (a) Isomer shifts for the Gd isotopes. (b) Isomer shifts for the Dy, Er, and Yb chains. (c) Isotope shifts for Gd. (d) Isotope shifts for the Dy, Er, and Yb isotopes. Data are from Ref. [20] except for the isotope shifts for Er and Yb nuclei which are extracted from Fig. 3 of Ref. [30]. The values of parameters β and γ in Eqs. (6) and (7) are given in the figure.

nuclei and the Yb and Hf chains, reflecting quite different sets of systematics between these two sets of nuclei. This will be discussed further in the next section.

IV. MAPPING THE SYMMETRY TRIANGLE

In order to quantitatively describe the IBA parameter space within the symmetry triangle, a coordinate system can be implemented (see for example Ref. [27]). We propose a simple set of polar coordinates to plot the IBA parameters within the triangle space. This mapping converts the parameters ζ and χ of Eq. (1) into radial and angular coordinates (ρ, θ) by

$$\rho = \frac{\sqrt{3}\zeta}{\sqrt{3}\cos\theta_\chi - \sin\theta_\chi},$$

$$\theta = \frac{\pi}{3} + \theta_\chi, \tag{8}$$

where $\theta_\chi = (2/\sqrt{7})\chi(\pi/3)$.

These coordinates allow for a convenient and simple description of the entire triangle, with θ ranging from 0° to 60° and ρ acting as a standard radial coordinate from 0 to 1. For example, $\rho=0$ for U(5), $\rho=1$, $\theta=0$ for SU(3), and $\rho=1$, $\theta=\pi/3$ for O(6). An illustration of these polar coordinates is included in Fig. 1.

With the identification of a set of parameters that provides a reasonable description of the evolution of the low-lying properties of the rare-earth nuclei, the trajectories of each isotopic chain can now be quantitatively mapped into the IBA triangle. The trajectories in the symmetry triangle corresponding to the fit parameters for the Gd-Hf isotopic chains are shown in Fig. 14 in terms of the polar coordinates defined in Eq. (8).

Inherent to the IBA model is a region of phase/shape coexistence [23,28]. As ζ is increased from zero, a first-order phase transition occurs as the nuclei evolve from spherical to deformed. This occurs for all χ values except for $\chi=0$, where the transition is second order. The region of phase/shape coexistence is included in Fig. 14 for $N_B=10$, corresponding to the typical boson number of nuclei in this region. The coexistence region varies to some extent with boson number and for larger boson number, moves slightly closer to the U(5) region of the triangle.

As N is first increased from the closed shell at $N=82$, all isotopic chains present an increasing quadrupole deformation [moving from U(5) towards the SU(3)-O(6) leg]. More specifically, all chains originate near the spherical, U(5) corner of the triangle, cross the phase/shape transition region, and continue into the deformed region. One very interesting feature of the evolution of each isotopic chain is that they all cross the phase transition region around neutron numbers 88 and 90.

In the phase transition region, larger Z values show increased γ-softness. For Gd, the first two nuclei in the chain are γ-stiff, lying on the U(5)-SU(3) leg of the triangle. The γ-softness increases slightly for the Dy and Er nuclei and even more so for the Yb and Hf nuclei, which lie very close

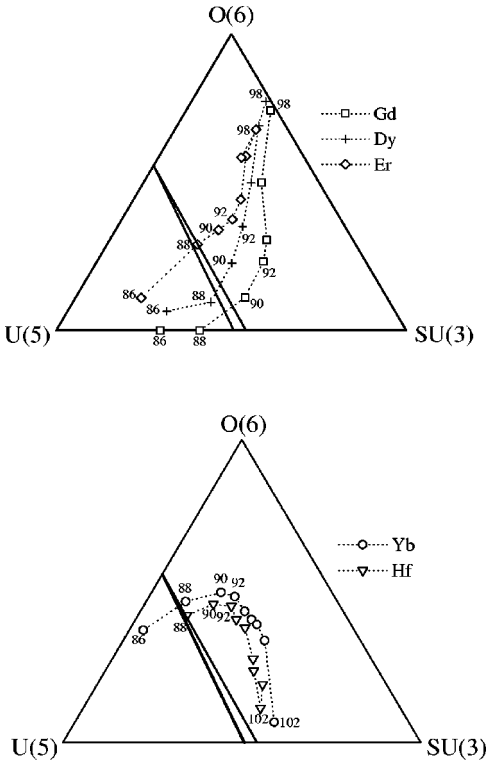

FIG. 14. Trajectories in the IBA symmetry triangle for the Gd-Hf isotopic chains. The slanting lines enclose the region of phase coexistence and phase transition corresponding to $N_B=10$.

to the U(5)-O(6) leg of the triangle. Going back to the observations on the behavior of $R_{4/2}$, S'_{2n}, $\delta\langle r^2\rangle$, and $\Delta\langle r^2\rangle^{(N)}$, it appears that for nuclei close to the U(5)-SU(3) leg of the triangle (axially symmetric), such as Gd and Dy, the manifestation of the transition from spherical to deformed is quite sudden, as evidenced by the sharp variation in the above observables. As Z is increased and the nuclei become more γ-soft, the more gradual evolution of $R_{4/2}$, S'_{2n}, $\delta\langle r^2\rangle$, and $\Delta\langle r^2\rangle^{(N)}$ suggests that the phase transition manifests itself less abruptly.

Past the phase transition region, the two groups take on quite different trajectories. The Gd, Dy, and Er isotopes show an increasing γ-softness and β deformation [closer to the O(6) limit with an increasing ζ]. The Yb and Hf isotopes present increasing γ-rigidity [moving toward the U(5)-SU(3) leg] with a constant β deformation. The different trajectories for Yb and Hf stem from and reflect (see Fig. 5) the low-lying 0_2^+ states in the heavier isotopes and the high γ-band energies. In contrast, Gd, Dy, and Er present the more typical situation in which the γ band is rather low lying at $\sim$1 MeV and the 0_2^+ excitation is somewhat higher.

V. CONCLUSION

Placing an equal emphasis on all low-lying, positive parity excitations, calculations were carried out for the $Z=64$ to 72, $N=86$ to 104 even-even rare-earth nuclei. They reproduce very well the energies of the bandheads and provide a reasonable description of the transition strengths. Other

quantities, such as two neutron separation energies, isomer and isotope shifts are also well described. Using a set of polar coordinates, the trajectory of each isotopic chain is mapped in the IBA symmetry triangle. It is observed that the isotopic chains break into two distinct trajectories, one containing the Gd, Dy, and Er isotopes, and the other consisting of the Yb and Hf isotopes. The results for Yb and Hf are quite different than previously obtained in calculations that gave less weight to the 0_2^+ levels. The different trajectories mirror the behavior of different observables, including $R_{4/2}$, $E(2_\gamma^+)$, $E(0_2^+)$, S'_{2n}, $\delta\langle r^2\rangle$, and $\Delta\langle r^2\rangle^{(N)}$.

ACKNOWLEDGMENTS

Useful discussions with F. Iachello, P. von Brentano, N. Pietralla, and R. Bijker are acknowledged. This work was supported by U.S. DOE Grant No. DE-FG02-91ER-40609 and by Contract No. Br799/11-1.

[1] A. Arima and F. Iachello, Phys. Rev. Lett. **35**, 1069 (1975).
[2] O. Scholten, F. Iachello, and A. Arima, Ann. Phys. (N.Y.) **115**, 325 (1978).
[3] A. Gómez, O. Castaños, and A. Frank, Nucl. Phys. **A589**, 267 (1995).
[4] J. E. García-Ramos, J. M. Arias, J. Barea, and A. Frank, Phys. Rev. C **68**, 024307 (2003).
[5] D. Bucurescu, G. Cata, D. Cutoiu, G. Constantinesu, M. Ivascu, and N. V. Zamfir, Z. Phys. A **324**, 387 (1986).
[6] W.-T. Chou, N. V. Zamfir, and R. F. Casten, Phys. Rev. C **56**, 829 (1997).
[7] F. Iachello, Phys. Rev. Lett. **85**, 3580 (2000).
[8] F. Iachello, Phys. Rev. Lett. **87**, 052502 (2001).
[9] R. F. Casten and N. V. Zamfir, Phys. Rev. Lett. **85**, 3584 (2000).
[10] R. F. Casten and N. V. Zamfir, Phys. Rev. Lett. **87**, 052503 (2001).
[11] P. O. Lipas, P. Toivonen, and D. D. Warner, Phys. Lett. **155B**, 295 (1985).
[12] N. V. Zamfir, P. von Brentano, R. F. Casten, and J. Jolie, Phys. Rev. C **66**, 021304(R) (2002).
[13] V. Werner, P. von Brentano, R. F. Casten, and J. Jolie, Phys. Lett. B **527**, 55 (2002).
[14] R. F. Casten and D. D. Warner, in *Progress in Particle and Nuclear Physics*, edited by D. Wilkinson (Pergamon, Oxford, 1983), Vol. 9, p. 311.
[15] R. Fossion, C. De Coster, J. E. Garcia-Ramos, T. Werner, and K. Heyde, Nucl. Phys. **A697**, 703 (2002).
[16] J. E. Garcia-Ramos, C. De Coster, R. Fossion, and K. Heyde, Nucl. Phys. **A688**, 735 (2001).
[17] M. A. Moinester, J. Alster, G. Azuelos, and A. E. L. Dieperink, Nucl. Phys. **A383**, 264 (1982).
[18] F. Iachello and A. Arima, *The Interacting Boson Model* (Cambridge University Press, Cambridge, 1987).
[19] F. Iachello and N. V. Zamfir Phys. Rev. Lett. (to be published).
[20] Nucl. Data Sheets, through Vol. 94, Issue 4 (2001).
[21] R. F. Casten and D. D. Warner, Rev. Mod. Phys. **60**, 389 (1988).
[22] R. F. Casten, P. von Brentano, and N. V. Zamfir, Phys. Rev. C **49**, 1940 (1994).
[23] A. E. L. Dieperink, O. Scholten, and F. Iachello, Phys. Rev. Lett. **44**, 1747 (1980).
[24] R. Bijker, A. E. L. Dieperink, and O. Scholten, Nucl. Phys. **A344**, 207 (1980).
[25] P. D. Duval and B. R. Barrett, Phys. Rev. C **23**, 492 (1980).
[26] P. Van Isacker and G. Puddu, Nucl. Phys. **A348**, 125 (1980).
[27] Y. Alhassid and N. Whelan, Phys. Rev. Lett. **67**, 816 (1991).
[28] F. Iachello, N. V. Zamfir, and R. F. Casten, Phys. Rev. Lett. **81**, 1191 (1998).
[29] E. A. McCutchan *et al.*, Phys. Rev. C **69**, 024308 (2004).
[30] G. D. Sprouse, J. Das, T. Lauritsen, J. Schecker, A. Berger, J. Billowes, C. H. Holbrow, H. E. Mahnke, and S. L. Rolston, Phys. Rev. Lett. **63**, 1463 (1989).